

Absolute measurement of the effective nonlinearities of KTP and BBO crystals by optical parametric amplification

D. J. Armstrong, W. J. Alford, T. D. Raymond, and A. V. Smith

Absolute magnitudes of the effective nonlinearity, d_{eff} , were measured for seven KTP and six BBO crystals. The d_{eff} 's were derived from the parametric gain of an 800-nm signal wave in the sample crystals when they were pumped by the frequency-doubled, spatially filtered light from an injection-seeded, Q -switched Nd:YAG laser. The KTP crystals, all type II phase matched with propagation in the X - Z plane, had d_{eff} values ranging from 1.97 to 3.50 pm/V. Measurements of gain as a function of phase velocity mismatch indicate that two of the KTP crystals clearly contain multiple ferroelectric domains. For five type I phase-matched BBO crystals, d_{eff} ranged from 1.76 to 1.83 pm/V, and a single type II phase-matched BBO crystal had a d_{eff} of 1.56 pm/V. The uncertainty in our measurements of d_{eff} values is $\pm 5\%$ for KTP and $\pm 10\%$ for BBO.

Key words: KTP crystals, BBO crystals, second-order nonlinear coefficients. © 1996 Optical Society of America

1. Introduction

KTP (KTiOPO_4) and BBO ($\beta\text{-BaB}_2\text{O}_4$) are two of the most widely used crystals in nonlinear optical devices because of their large transparency ranges, relatively high nonlinearities, and high damage thresholds. There have been numerous absolute and relative measurements of the second-order nonlinear optical coefficients of KTP¹⁻¹⁰ and BBO.^{2,11-13} (Ref. 10 lists nonlinear coefficients for many crystals and discusses IEEE/ANSI Std. 176 relating to nonlinear crystal nomenclature.) In this paper we report our absolute measurements of the magnitude of the effective nonlinearity, d_{eff} , for several samples of these two crystals. We were motivated to do so by the large variations we found in the performance of optical parametric oscillators (OPO's) for a selection of KTP crystals that were supposed to be identical. For example, we found that the OPO oscillation threshold required pump powers that differed by as much as a factor of 4 when supposedly identical

crystals were placed in the same OPO cavity. This led us to suspect that not all KTP crystals are created equal. We report here confirmation of this suspicion by demonstrating that nominally identical KTP crystals can have substantially different d_{eff} 's. This may explain in part the varying values of nonlinear coefficients reported in the literature for KTP. For example, the d_{ij} 's reported in Refs. 6, 7, and 10 give magnitudes for d_{eff} of approximately 3.7, 2.26, and 3.1 pm/V, respectively, for the pump wavelength and the signal wavelength we used. Of the seven KTP crystals we tested, one had a d_{eff} that agreed well with the value derived from Ref. 10, one had a relatively large d_{eff} near the value derived from Ref. 6, and the rest had smaller d_{eff} 's closer to the value derived from Ref. 7. Although we initially concentrated on KTP, our experimental setup also permitted measurement of d_{eff} for several BBO crystals to test their uniformity and compare their coefficients with previously measured values.

Second-order nonlinear optical coefficients can be measured by a variety of methods, including the Maker fringe technique,^{14,15} phase-matched second-harmonic generation with pulsed¹⁶ and cw¹⁷⁻¹⁹ lasers, surface second harmonics,^{20,21} and parametric fluorescence.^{22,23} These methods were first demonstrated at least 25 years ago, and although improvements have been made over the years, each has

The authors are with the Department of Lasers, Optics, and Remote Sensing, Sandia National Laboratories, Albuquerque, New Mexico 87185-1423.

Received 3 August 1995; revised manuscript received 20 November 1995.

0003-6935/96/122032-09\$06.00/0

© 1996 Optical Society of America

advantages and disadvantages. The Maker fringe technique, utilizing non-phase-matched second-harmonic generation, determines the sign and magnitude of second-harmonic coefficients and became a standard following the research of Jerphagnon and Kurtz.¹⁵ Initially, absorptive and anisotropic properties were neglected, resulting in errors in measurements of d_{ij} . Recently, they have been included,²⁴ so the Maker fringe technique is now applicable to most crystal classes. Measuring d_{eff} by the use of phase-matched second-harmonic generation remains popular,² but cw measurements involve focused beams²⁵ and require complex mathematical extraction of d_{eff} . Surface second-harmonic generation is best suited for determining d_{ij} in highly absorptive materials, and parametric fluorescence returns d_{ij} values that are consistently larger than those determined by other methods for reasons that are not well understood (see Ref. 9 and references therein). The method of parametric amplification that we employ has the advantage of directly determining d_{eff} for crystals cut to phase match at wavelengths other than the second harmonic of the pump.

The KTP crystals we tested were type II phase matched with light propagating in the X - Z plane at an angle of $\theta = 58.6^\circ$. The 532-nm pump light was o polarized, the 800-nm signal light was e polarized, and the resulting 1588-nm idler light was o polarized. For this process, d_{eff} is related to the nonlinear susceptibility tensor elements by $d_{\text{eff}} = d_{32} \sin \theta$. The type I BBO crystals were cut near $\theta = 22.2^\circ$, the phase-matching angle for 532 nm (e), 800 nm (o), and 1588 nm (o). Here, $d_{\text{eff}} = d_{31} \sin \theta - d_{22} \cos \theta$. For type II mixing in BBO with 532 nm (e), 800 nm (o), and 1588 nm (e), the phase-matching angle is 26.6° and $d_{\text{eff}} = d_{22} \cos^2 \theta$.

Our measurement technique is based on parametric amplification of light from a cw laser in a sample crystal that is pumped by the spatially filtered second-harmonic light from an injection-seeded, Q -switched Nd:YAG laser. Gain is measured only over the central region of a large-diameter, highly collimated pump beam that has a smooth spatial irradiance distribution. In addition, the gain is sampled only at the peaks of the pump and signal pulses. Together these conditions guarantee that the pump irradiance is nearly spatially and temporally uniform over the measured region, so corrections for nonuniform pumping are minimized. The analysis was thus straightforward and consisted of extracting d_{eff} from a nonlinear least-squares fit to measurements of gain versus pump irradiance. The experiment is described in more detail in Section 2, and our analysis of the data is discussed in Section 3.

KTP is a ferroelectric crystal, so multiple domains can exist within a single crystal.²⁶ Polarity-reversed domains are not evident in a crystal's linear optical properties, but since the sign of d_{eff} is reversed, multiple polarity-reversed domains can be detected by the measurement of signal gain as a

function of phase velocity mismatch Δk , where $\Delta k = k_{\text{pump}} - k_{\text{signal}} - k_{\text{idler}}$. In the laboratory, we measured parametric gain as a function of crystal angle near the phase-matching angle. For a crystal of total length L with n domains of equal length, these phase-matching curves have characteristic profiles with $n - 2$ small peaks lying between two large peaks of equal height separated by $\Delta kL/\pi \lesssim 2n$. With unequal length domains, the shape of the phase-matching curve depends on the lengths and ordering of the domains but can be dominated by a broadened single peak. From these signatures, we demonstrated that at least three of the KTP crystals with the lowest d_{eff} 's have polarity-reversed multiple ferroelectric domains.

2. Method of Measurement

With pump depletion and linear absorption neglected, the parametric gain of an incident signal field, $E_s(0)$, in the absence of an incident idler field is given in SI units by^{27,28}

$$E_s(L) = E_s(0) \left(\cosh gL - \frac{i\Delta k}{2g} \sinh gL \right) \exp(i\Delta kL/2), \quad (1)$$

where

$$g = [\Gamma^2 - (\Delta k/2)^2]^{1/2}, \quad (2)$$

Δk is the phase velocity mismatch,

$$\Delta k = k_p - k_s - k_i, \quad (3)$$

$$\Gamma^2 = \frac{2|d_{\text{eff}}|^2 w_s w_i I_p}{\epsilon_0 n_s n_i n_p c^3}. \quad (4)$$

The subscripts s , i , and p denote the signal, idler, and pump waves, respectively, with $I_p = n_p \epsilon_0 c |E_p|^2/2$ being the pump irradiance (W/m^2), n_s , n_i , and n_p the refractive indices, ϵ_0 the permittivity of free space, L the crystal length, and c the speed of light. Our method of measuring d_{eff} relied on an accurate determination of the signal gain, $|E_s(L)|^2/|E_s(0)|^2$, as a function of the pump irradiance I_p . From these data, Eq. (1) is used to deduce best values for Γ and Δk . Equation (4) then gives the value of d_{eff} .

A diagram of the experimental setup is shown in Fig. 1. The beam from an 800-nm single-longitudinal-mode cw diode laser (SDL AR-5412-H1) was amplified by parametric mixing with the frequency-doubled, 8-ns (FWHM) light pulse from an injection-seeded, Q -switched Nd:YAG laser (Continuum NY 82-10). Spatial filtering of both beams, by focusing them through diamond pinholes, produced smooth irradiance profiles. An iris diaphragm allowed only the central disk of the resulting pump beam Airy pattern to reach the crystal, so the pump distribution within the crystal was well known. In the crystal, the pump and signal beams were highly collimated (beam divergence angles \ll phase-matching acceptance angles) with typical $1/e^2$ irradiance

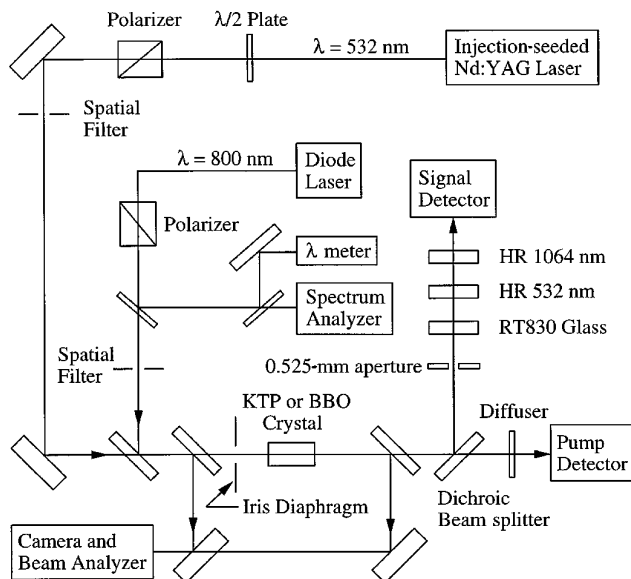


Fig. 1. Diagram of parametric gain experiment used to make absolute measurements of d_{eff} for KTP and BBO. HR, highly reflective.

diameters of 2.5 mm and 1.5 mm, respectively. Their irradiance profiles and beam diameters were monitored by a CCD camera-based laser beam profiler. Least-squares fits of the fluence spatial profiles to Gaussian profiles typically returned correlation coefficients $\geq 96\%$ for the pump and signal beams. The amplified signal was measured only over a small central portion of the pump beam, where the pump irradiance and thus the signal amplification were nearly uniform. This was accomplished by insertion of a 0.525-mm-diameter aperture in the signal beam after it was separated from the pump light. We took care to ensure that the 800-nm signal alone reached the signal detector. Any pump, idler, or Nd:YAG fundamental light remaining after the dichroic beam splitter was rejected by a Hoya RT-830 colored glass filter ($T_{532 \text{ nm}} < 0.01$, $T_{800 \text{ nm}} \approx 0.85$, $T_{1064 \text{ nm}} \approx 0.50$, $T_{1588 \text{ nm}} < 0.01$), followed by high reflectors for 532 and 1064 nm.

The injection-seeded Nd:YAG laser generated temporally smooth pulses. Peak values of the pump and amplified signal pulses were time selected by the use of fast samplers with 200-ps gates (SRS SR-255) centered on the peak of the pulses. Data consisted of the unamplified cw signal irradiance, the peak amplified signal irradiance, and the transmitted 532-nm pump energy. The pump energy was combined with the measured spatial and temporal pump profiles to deduce the pump irradiance at the center of the pump beam. The transmitted pump energy provided a reliable measure of the pump energy within the crystal when the exit face reflective losses were accounted for. (Exit face reflective losses were neglected for antireflection coated crystals.) Measuring transmitted energy avoids the need to account for étalon effects that occur in angle-tuned

crystals with parallel faces. We observed approximately 10% modulations (étalon effects) on the transmitted pump beam energy during angle tuning of the crystal, even for some crystals that were antireflection coated.

The pump detector had a bandwidth of >1 GHz (Hamamatsu R1328U-02) and was calibrated against a calibrated joule meter (Scientech 380101) with the nonlinear crystal removed from the pump beam path. Because the pump detector measured the energy sampled by a 200-ps gate and the joule meter measured the total pulse energy, calibration required knowledge of the pulse shape. This was determined by scanning of the 200-ps gate across the pulse to record the time profile. The digitized pulse profile was subsequently integrated, and the pulse and gate areas were compared to determine the fraction of pump energy in the gate. Gate scanning was also used to determine the delays required for coincidence of the 200-ps gates with the peaks of the signal and pump pulses. The data-acquisition system was triggered on the rising edge of the pump pulse with a constant fraction discriminator and 200-ps rise time photodiode. The pump and signal pulse profiles were periodically scanned to ensure coincidence of the 200-ps gates with the pulse peaks, and the pump profile was periodically recorded to monitor any changes in the pulse shape.

The unamplified signal irradiance was recorded at the signal detector during the 200-ps gate with the pump beam blocked by a mechanical shutter. The signal power incident upon the crystal was typically 30 mW, but at the signal detector it was only 2–3 mW. The signal detector (New Focus 1611) had a bandwidth of 1 GHz and generated ~ 40 mV dc for the unamplified signal. The maximum signal amplification was typically ≤ 15 , so the maximum signal pulse energies were ≤ 10 nJ. With the maximum pump pulse energies typically exceeding 15 mJ, pump depletion was negligible.

Phase matching was controlled by rotation of the crystal with stepping motors through various reduction gears, giving internal angle resolutions of 28.4 μrad for BBO, and either 43.6 or 25.9 μrad for KTP. Acceptance angles for the KTP, type II BBO, and type I BBO were 0.93, 0.74, and 0.59 mrad cm, respectively. The crystal lengths ranged from 7.24 to 10.54 mm, so the angular resolution was more than sufficient for these measurements.

In preparation for data collection, the crystal was removed and the pump and signal beams were carefully collimated and overlapped by observation of beam profiles at two points either side of where the crystal normally resides. The crystal was then replaced and rotated for large signal amplification, and the 0.525-mm-diameter aperture was placed in the signal beam. The aperture was positioned to sample that portion of the signal beam with maximum gain. Several iterations of crystal rotation, followed by aperture position adjustments, were

required for optimization of the signal gain. Data collection consisted of adjustment of the pump pulse energy with a half-wave plate and linear polarizer placed upstream from the pump beam spatial filter, and recording of the peak amplified signal irradiance and total pump energy for each pump pulse. There was no observable change in the pump beam's spatial irradiance profile as the pump pulse energy was varied. A typical data set began with one measurement of baseline noise and one cw signal irradiance measurement, followed by 200–400 data points.

The extraordinary beam walk-off angles are 49 mrad, 48 mrad, and 55 mrad, respectively, for KTP, type I BBO, and type II BBO. For the longest crystal used in these measurements, the resulting extraordinary beam displacement was ≤ 0.58 mm. Ideally, our pump beam diameter would be much larger than this displacement, but it was limited by the available power and by the 5 mm \times 5 mm crystal faces. At 2.5 mm, our pump beam diameter was substantially larger than the walk-off, and we show in Section 3 that walk-off had little impact on our results.

3. Analysis and Results

The raw experimental data consisted of the dc signal level, the peak amplified signal, and the transmitted pump energy. To derive d_{eff} from these data we calculated the peak pump irradiance and the peak signal gain. The data were then fitted to Eq. (1) by the nonlinear least-squares-fit algorithm of Marquardt²⁹ to find the best values for Γ and Δk , from which d_{eff} can be determined. As a starting point for the fitting routine, we used a small value of Δk and an estimate of Γ from the data point with the highest measured I_p , where $\text{gain} \approx \cosh^2 \Gamma L \approx 1/2 + 1/4 \exp(2\Gamma L)$. The fit routine returned Δk directly, whereas d_{eff} was extracted from the returned value of Γ by the use of known values for the refractive indices. The fit routine was thoroughly tested with simulated data for a large range of d_{eff} and Δk values. Figure 2(a) shows typical signal gain data and the least-squares-fit for crystal KTP-3, plotted against $\sqrt{I_p}$. Figure 2(b) shows the same for crystal BBO-5.

In analyzing the accuracy of our method we must consider that the pump irradiance is not truly uniform over the sampled gain region, and that walk-off might influence our results. In addition, the KTP crystals could suffer minor photochromic damage, leading to an increase in absorption, and could have multiple ferroelectric domains. Each of these topics is addressed here and our best values for d_{eff} for each crystal are tabulated.

First we consider the conversion from pump energy to peak pump irradiance. Gain was measured only over the central 0.525-mm-diameter portion of the pump beam. We determine the average irradiance in this region by taking the product of the total pump energy, the ratio of gate area to pulse area, the fraction of pump energy contained in the gain region,

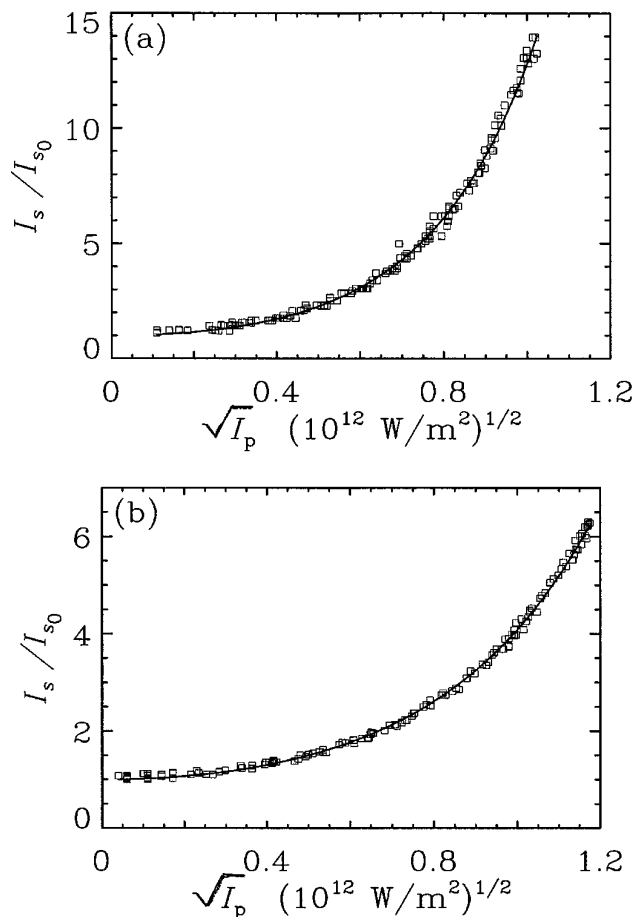


Fig. 2. (a) Typical signal gain data (squares) plotted against the square root of pump irradiance I_p with the least-squares fit (solid curves) for KTP-3. (b) Typical data with the least-squares fit for BBO-5.

and then dividing by the area of the pump region and by the gate width of 200 ps. We find the fraction of energy in the gain region by assuming a Gaussian beam profile with the measured radius, integrating it over the apertured gain region, and dividing by the integral over the full beam profile. We then adjust I_p for reflective loss, with $R = [(n_p - n_{\text{air}})/(n_p + n_{\text{air}})]^2$ at the exit face for crystals that were not antireflection coated. Figure 3 depicts graphically the quantities involved in determining I_p by showing (a) a 200-ps gate superposed on a typical pulse profile, (b) a measured pump irradiance profile, and (c) the 0.525-mm-diameter Gaussian cap on a pump beam profile calculated with the measured beam diameter. As mentioned above and as shown in Figs. 3(b) and 3(c), Gaussian profiles are a close approximation of the experimental beam profiles. An alternative way to determine the volume fraction is to place an aperture in the pump beam as well. Measurements of energy transmitted through small apertures of various diameters confirmed our calculated transmitted energy fractions.

Because the pump irradiance varied somewhat over the gain area, we must consider what correc-

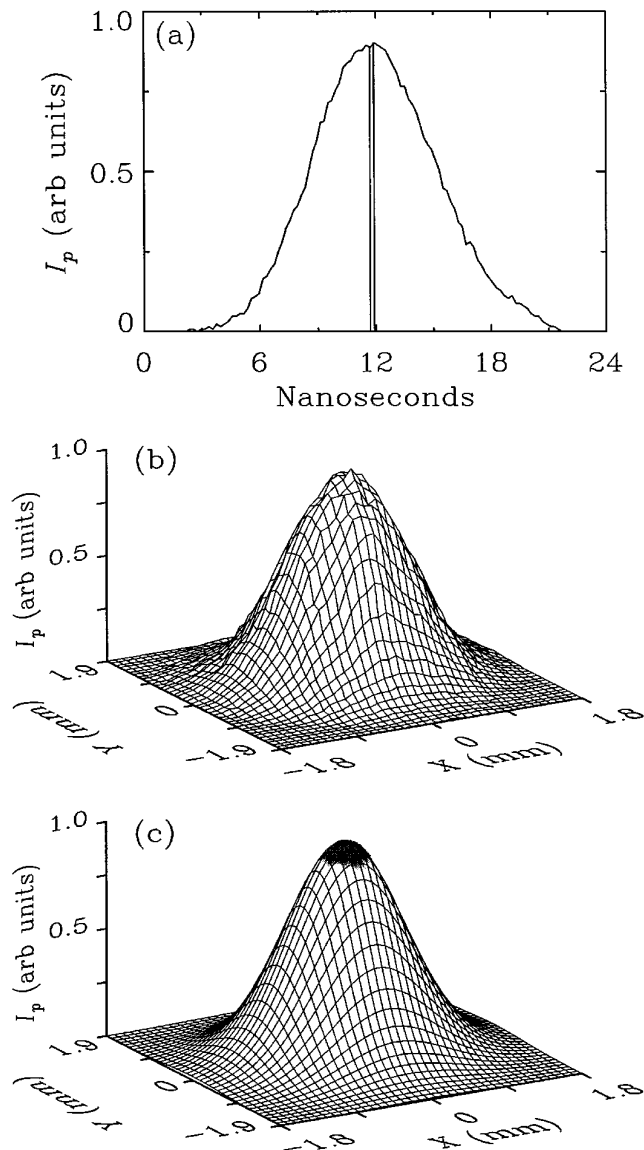


Fig. 3. Quantities involved in determining the peak pump irradiance: (a) 200-ps gate superposed on a typical pump pulse with a FWHM of 8 ns, (b) measured pump beam irradiance profile, (c) 0.525-mm-diameter Gaussian cap on a pump beam profile calculated with the measured beam diameter (the cap denotes the top of the cylindrical volume of pump energy that mixed with and amplified the signal beam).

tions should be made in deriving d_{eff} . For our pump beam with a $1/e^2$ diameter of 2.5 mm, I_p is 8.5% smaller at the edge of the 0.525-mm aperture than at the center. To determine how much this influences d_{eff} , we synthesized data consisting of the average gain versus the pump irradiance averaged over the aperture for $\Delta k = 0$. With the signal irradiance given by

$$I_s = I_{s_0} \exp[-2(r/b)^2], \quad (5)$$

and the pump irradiance given by

$$I_p = I_{p_0} \exp[-2(r/a)^2], \quad (6)$$

the expression for the average gain is

$$G_{\text{av}} = \frac{\int_0^R \exp[-2(r/b)^2] \cosh^2[\Gamma_0 L \exp[-(r/a)^2]] 2\pi r dr}{\int_0^R \exp[-2(r/b)^2] 2\pi r dr}, \quad (7)$$

where b is the radius of the signal beam (0.75 mm), a is the radius of the pump beam (1.25 mm), R is the radius of the aperture (0.2625 mm), and Γ_0 is Γ at the center of the pump beam. When d_{eff} was extracted from this simulated data by the use of our usual procedure, it was 0.6% lower than the actual value. Thus the variation of pump and signal irradiance over the sampled aperture has a negligible effect on the measured values of d_{eff} . Of course, for larger apertures the discrepancy would increase and corrections would be necessary. In addition, the value of Δk required to fit the data increases with the aperture size.

As mentioned in Section 1, birefringent walk-off was relatively unimportant in our measurements because the pump beam diameter was several times greater than the walk-off displacement. We investigated its influence on the measured value of d_{eff} experimentally and by numerical modeling. The usual measurement with overlapped pump and signal beam axes was made first; then the extraordinary signal beam was offset relative to the ordinary pump beam by 1/2 the walk-off displacement (~ 0.25 mm) to compensate for walk-off. The 0.525-mm aperture was readjusted for maximum gain and d_{eff} was remeasured. After several trial measurements of this type, the difference in d_{eff} for the displaced and centered signal beam was $< 4\%$. A numerical simulation that included Gaussian beam profiles and walk-off^{30,31} yielded results similar to the experiment. A baseline calculation without walk-off was made first, using typical experimental parameters. When walk-off was added to the calculation, the signal gain was found to drop 4%. The 4% reduction in gain translates into a reduction in d_{eff} of only 1.5%. When the incident signal beam was displaced to compensate for walk-off, the signal gain was 1.5% lower than the baseline calculation. Because measured and numerically modeled walk-off effects were small, we made all subsequent measurements with the beam centers overlapped.

Another potential source of error is pump and signal absorption caused by laser-induced photochromic damage. This effect has been observed in KTP with peak irradiances comparable with the largest peak irradiance used in our measurements.^{32,33} To determine what effect photochromic damage may have had, we exposed KTP-4 (a multiple-domain crystal) to high peak pump irradiances for extended time periods and monitored the incident and transmitted pump energy. To facilitate observation of

photochromic damage and any subsequent absorption, we increased I_p by reducing the pump beam diameter to 1 mm ($1/e^2$) and sampled the central portion of the transmitted beam through a 0.320-mm aperture placed beyond the crystal. With pump fluences of 0.88, 1.26, and 1.93 J/cm² (peak on-axis irradiances of 1.2×10^{12} , 1.7×10^{12} , and 2.6×10^{12} W/m², respectively), we observed no increase in pump absorption and no visible damage (i.e., gray tracks) after approximately 6000 laser pulses. With a pump fluence of 2.54 J/cm² (peak on-axis irradiance of 3.4×10^{12} W/m²), we observed $\sim 2\%$ reduction in the ratio of transmitted to incident pump energy, and barely visible gray tracks, after 3700 laser pulses. With no further exposure, the gray tracks became unobservable after approximately 12 h at room temperature. In the course of a typical d_{eff} measurement (i.e., optimize signal gain and collect several data sets), a KTP crystal was exposed to perhaps several thousand pulses at most with fluence ≥ 0.78 J/cm² ($\sim 1.0 \times 10^{12}$ W/m²), as shown in Fig. 2(a). During the remainder of the measurement the crystal was exposed to fluences ≤ 0.6 J/cm². Although we performed a simple series of tests on just one of seven KTP crystals, we concluded that photochromic damage, and any resulting absorption, had no effect on our results.

Measured values of d_{eff} for the KTP and BBO crystals are shown in Tables 1 and 2, respectively. As Table 1 shows, there is a wide variation in d_{eff} for KTP. Of the seven tested, KTP-3 was the only KTP crystal whose d_{eff} nearly matched a previously reported value of 3.07 pm/V.¹⁰ Perhaps more important, it produced the most consistent data: Its measured phase mismatch Δk , and the standard deviations in the fit parameters, $\sigma_{d_{\text{eff}}}$ and $\sigma_{\Delta k}$, were very small. (Typically, $\sigma_{d_{\text{eff}}}/d_{\text{eff}} < 0.01$ and $\sigma_{\Delta k}/\Delta k < 0.1$ for KTP-3.) KTP-2 had a measured d_{eff} of 2.92 pm/V, within 5% of that given in Ref. 10, and it also produced data with small $\sigma_{d_{\text{eff}}}$ and $\sigma_{\Delta k}$. KTP-5, the only hydrothermally grown crystal we tested, had the highest measured d_{eff} of 3.50 pm/V.

Table 1. Measured d_{eff} Values of KTP Crystals for the Mixing Process 532 nm (o) \rightarrow 800 nm (e) + 1588 nm (o), with Phase-Matching Angle $\theta = 58.6^\circ$ in the X-Z Plane

Crystal ^a	Supplier	d_{eff} (pm/V)
KTP-1	JTT	2.58 ± 0.13
KTP-2	Phillips	2.92 ± 0.15
KTP-3	Phillips	3.05 ± 0.15
KTP-4 ^b	Phillips	1.99 ± 0.10
KTP-5 ^c	Litton	3.50 ± 0.18
KTP-6	Phillips	2.17 ± 0.11
KTP-7 ^d	Phillips	1.97 ± 0.10

^aAll Phillips crystals and the JTT crystal were flux grown. KTP-5, supplied by Litton, was hydrothermally grown.

^bMultiple ferroelectric domains.

^cTransmitted signal and pump wave fronts were significantly distorted by KTP-5. The value of $d_{\text{eff}} = 3.50$ is considered unreliable. See text for additional details.

^dMultiple ferroelectric domains.

Table 2. Measured d_{eff} Values for BBO Crystals

Crystal ^a	d_{eff} (pm/V)
BBO-1	1.76 ± 0.18
BBO-2	1.83 ± 0.18
BBO-3	1.82 ± 0.18
BBO-4	1.83 ± 0.18
BBO-5	1.85 ± 0.19
BBO-6	1.56 ± 0.16

^aBBO-1–BBO-5 are type I phase matched at $\theta = 22.2^\circ$ for the mixing process 532 nm (e) \rightarrow 800 nm (o) + 1588 nm (o). BBO-6 is type II phase matched at $\theta = 26.6^\circ$ for the mixing process 532 nm (e) \rightarrow 800 nm (o) + 1588 nm (e). All crystals were supplied by Cleveland Crystals, Inc.

However, this crystal significantly distorted the pump and signal wave fronts without affecting the polarization of either. Because the measurement was made with distorted irradiance profiles, we consider its d_{eff} to be less reliable than the others. Crystals KTP-4 and KTP-7 have the lowest d_{eff} 's. Their phase-matching curves, each with two distinct peaks, reveal that these crystals have multiple ferroelectric domains. For these two crystals, d_{eff} was measured at the points in their phase-matching curves where gain was maximum. Finally, KTP-1 and KTP-6 have single-peaked phase-matching curves, but d_{eff} 's approximately 15% and 29% lower, respectively, than the value of Ref. 10. Although single peaked, the width of the phase-matching curve for KTP-6 was approximately twice that expected for a single-domain crystal. The additional width suggests a multiple-domain structure.

In Fig. 4, we plot measured (boxes) and calculated (solid curves) phase-matching curves for (a) KTP-3, (b) KTP-4, and (c) KTP-7. These are plots of signal gain, $I_s/I_s(0)$ versus $\Delta kL/\pi$ for fixed pump power. For a single-domain crystal, the phase-matching curve can be calculated from Eq. (1). For a multiple-domain crystal, idler is generated in the first domain and mixes with the pump and signal in each successive domain. In this case, calculation of the phase-matching curve requires the two coupled equations for the signal and for the idler,^{27,28}

$$E_s(L') = E_s(0) \left(\cosh gL' - \frac{i\Delta k}{2g} \sinh gL' \right) \exp(i\Delta kL'/2) + i \frac{\kappa_1 E_p E_i^*(0)}{g} (\sinh gL') \exp(i\Delta kL'/2), \quad (8)$$

$$E_i(L') = E_i(0) \left(\cosh gL' - \frac{i\Delta k}{2g} \sinh gL' \right) \exp(i\Delta kL'/2) + i \frac{\kappa_2 E_p E_s^*(0)}{g} (\sinh gL') \exp(i\Delta kL'/2), \quad (9)$$

respectively, where

$$\kappa_i = \frac{d_{\text{eff}} w_i}{n_i c} \quad (10)$$

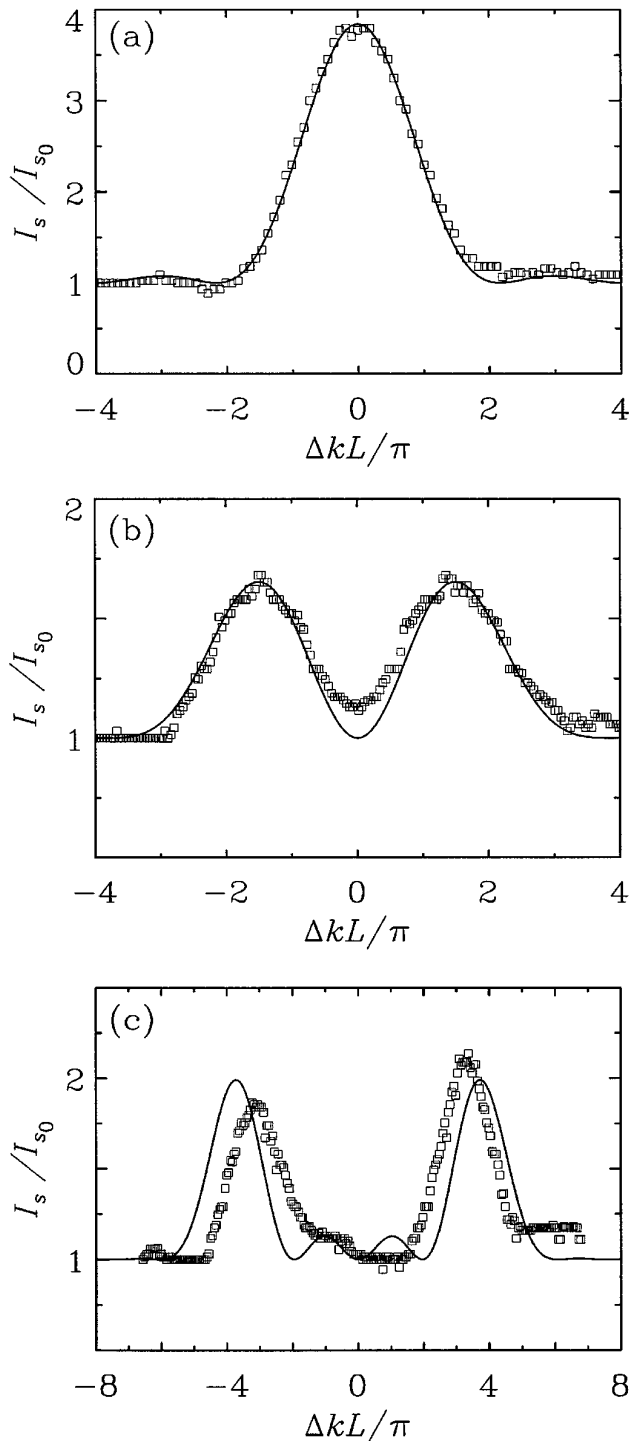


Fig. 4. Measured (boxes) and calculated (solid curves) signal gain as a function of $\Delta kL/\pi$ for (a) KTP-3, a crystal with a single ferroelectric domain; (b) KTP-4, assuming two equal length domains; (c) KTP-7, assuming four equal length domains. See text for additional details.

and L' is a domain length. Assuming equal length domains, with sign-reversed d_{eff} 's but constant Δk , iteration of Eqs. (8) and (9) for two domains gives the curve shown in Fig. 4(b). For four domains, the curve is shown in Fig. 4(c). [Note that a relative phase shift of $\Delta kL'$ caused by linear propagation was

factored out of the mixing equations in deriving Eqs. (8) and (9), i.e., ΔkL in Eq. (1), so the signal or idler phase should be shifted by that amount before iterating for the next domain.] The shapes of calculated phase-matching curves in Figs. 4(b) and 4(c) are not expected to match perfectly because the domains are not likely to have equal lengths. Nevertheless, it is clear that KTP-4 has two domains of comparable length, and KTP-7 probably has four domains. The curves in Figs. 4(b) and 4(c) were calculated with $d_{\text{eff}} = 3.0$ pm/V with the pump irradiance adjusted for the best fit. Because the domains are likely to have unequal lengths, we did not try to determine d_{eff} for KTP from the multiple-domain fits to the measured phase-matching curves of KTP-4 and KTP-7.

The broadened single-peaked phase-matching curve observed for KTP-6 can be reproduced from Eqs. (8) and (9) by consideration of multiple domains of unequal length. For example, with the assumption of $d_{\text{eff}} = 3.0$ pm/V, a calculated single-peaked curve with peak gain equal to the measured gain for a known I_p was obtained with domains of 8.75 and 1.25 mm for this 10-mm-long crystal. Although this calculated curve matched the shape of our measured curve quite well, the number of polarity-reversed domains and their lengths probably cannot be determined with high accuracy from parametric gain data. (The measured shape can be matched with more than two domains, but the additional domains must be ≤ 0.2 mm.) On the other hand, second-harmonic generation in the low conversion limit,³⁴ with characteristic $\text{sinc}^2(\Delta kL/2)$ phase-matching curves, might yield more accurate results. With low-conversion second-harmonic generation, the Fourier transform of the second-harmonic field $E(2\omega)$ reproduces the domain structure.

Unlike KTP, BBO is not ferroelectric. All the BBO crystals are single domain, and the d_{eff} values for the type I crystals, BBO-1–BBO-5, shown in Table 2 are quite consistent. However, all the BBO crystals, including the type II BBO-6, have d_{eff} 's approximately 10% lower than the values of 2.07 pm/V for type I, and 1.76 pm/V for type II, derived from the d_{ij} given in Ref. 10. This discrepancy might be associated with a consistently large value of Δk returned by the fit routine for all of the data for BBO. Although it is difficult to exactly locate the $\Delta k = 0$ angle when gain measurements are made, our fits to the BBO data returned Δk values that seemed physically unreasonable. For example, most of the KTP data (excluding KTP-5) had $\Delta kL/\pi \leq 0.3$, implying that the crystal angle was adjusted close to the peak of the phase-matching curve [e.g., see Fig. 4(a)]. On the other hand, most of the BBO data had $0.6 \leq \Delta kL/\pi \leq 0.8$, which from Fig. 4(a) would imply a substantial reduction in gain. The reduced gain associated with such a large Δk should have been noticeable while we were optimizing the gain. Although the Δk 's for BBO were consistently large, they were not always statistically significant. In

many measurements the standard deviation, $\sigma_{\Delta k}$, in the fit to Δk , was comparable with Δk .

We were not able to identify any systematic problem with our measurement method that would explain this difference between the KTP and BBO data, so we do not know if it indicates a problem with the BBO crystals or with our methods. One difference between the BBO and KTP samples was that the BBO crystals were not antireflection coated. This means the signal and idler waves resonate in the cavity formed by the two parallel end faces of the crystal. We tested by numerical modeling^{30,31} whether this could mimic a spurious Δk and found the effect was much too small to account for the best fit values of Δk .

After adding up uncertainties caused by spatial beam profiles, energy calibration, birefringent walk-off, and reflections at the crystal faces, we conservatively estimate the accuracy of the d_{eff} measurements for KTP to be $\pm 5\%$ (except KTP-5, which has large wave-front distortions as discussed above.) Since the BBO data suggest the possibility of a systematic effect that remains unexplained, the accuracy of the d_{eff} measurements for BBO is assumed to be lower than for KTP. We estimate the uncertainty for BBO to be $\pm 10\%$.

4. Conclusion

We made absolute measurements of effective nonlinearity d_{eff} for seven KTP crystals, five type I BBO crystals, and one type II BBO crystal. The measurements were based on pulsed optical parametric amplification of a cw laser. Highly collimated, spatially smooth pump and signal beams, and a temporally smooth pump pulse allowed very accurate determination of peak pump irradiance and peak signal gain. Analysis of the data was simple and consisted of extracting d_{eff} and Δk from curves of peak signal gain as a function of peak pump irradiance.

The measurements were motivated by our observations of widely varying OPO oscillation thresholds when different KTP crystals were placed in the same OPO cavity. The results demonstrated that KTP crystals can have widely varying values of d_{eff} . When systematic effects are accounted for, the accuracy of the d_{eff} measurements for KTP is estimated to be $\pm 5\%$. In addition, measurements of signal gain as a function of phase mismatch showed that at least three out of the seven commercially grown KTP crystals had multiple ferroelectric domains. These KTP crystals were purchased 2 to 3 years ago and may not reflect the quality and consistency of crystals available today.

The measurements of d_{eff} for BBO suggest much greater consistency in the quality of the BBO crystals. Although the variations in d_{eff} for the five type I BBO crystals were $<4\%$, the BBO data also suggest a still-unexplained systematic effect that somehow affects our measured values for Δk . The uncertainty in the BBO measurements is therefore higher than for KTP and is estimated to be $\pm 10\%$.

This research was supported by the U.S. Department of Energy under contract DE-AC04-94AL85000.

References

1. J. D. Bierlein and H. Vanherzeele, "Potassium titanyl phosphate: properties and new applications," *J. Opt. Soc. Am. B* **6**, 622–633 (1989).
2. R. C. Eckardt, H. Masuda, Y. X. Fan, and R. L. Byer, "Absolute and relative nonlinear optical coefficients of KDP, KD*P, BaB₂O₄, LiIO₃, MgO:LiNbO₃, and KTP measured by phase-matched second-harmonic generation," *IEEE J. Quantum Electron.* **26**, 922–933 (1990).
3. K. Kato, "Parametric oscillation at 3.2 μm in KTP pumped at 1.064 μm ," *IEEE J. Quantum Electron.* **27**, 1137–1140 (1991).
4. K. Asaumi, "Second-harmonic power of KTiOPO₄ with double refraction," *Appl. Phys. B* **54**, 265–270 (1992).
5. R. DeSalvo, D. J. Hagan, M. Sheik-Bahae, G. Stegeman, E. W. Van Stryland, and H. Vanherzeele, "Self-focusing and self-defocusing by cascaded second-order effects in KTP," *Opt. Lett.* **17**, 28–30 (1992).
6. H. Vanherzeele and J. D. Bierlein, "Magnitude of the nonlinear-optical coefficients of KTiOPO₄," *Opt. Lett.* **17**, 982–984 (1992).
7. B. Boulanger, J. P. Fève, G. Marnier, B. Ménaert, X. Cabirol, P. Villeval, and C. Bonnin, "Relative sign and absolute magnitude of $d^{(2)}$ nonlinear coefficients of KTP from second-harmonic-generation measurements," *J. Opt. Soc. Am. B* **11**, 750–757 (1994).
8. J.-J. Zondy, M. Abed, and A. Clairon, "Type-II frequency doubling at $\lambda = 1.30 \mu\text{m}$ and $\lambda = 2.53 \mu\text{m}$ in flux-grown potassium titanyl phosphate," *J. Opt. Soc. Am. B* **11**, 2004–2015 (1994).
9. E. C. Cheung, K. Koch, G. T. Moore, and J. M. Liu, "Measurements of second-order nonlinear optical coefficients from spectral brightness of parametric fluorescence," *Opt. Lett.* **19**, 168–170 (1994).
10. D. A. Roberts, "Simplified characterization of uniaxial and biaxial nonlinear crystals: a plea for standardization of nomenclature and conventions," *IEEE J. Quantum Electron.* **28**, 2057–2074 (1992).
11. C. Chen, B. Wu, A. Jiang, and G. You, "A new type ultraviolet SHG crystal $\beta\text{-BaB}_2\text{O}_4$," *Sci. Sin. Ser. B* **28**, 235–243 (1985).
12. C.-T. Chen, Y. X. Fan, R. C. Eckardt, and R. L. Byer, "Recent developments in barium borate," in *Laser and Nonlinear Optical Materials*, L. G. DeShazer, ed., *Proc. SPIE*, **681**, 12 (1986).
13. D. Eimerl, L. Davis, S. Velsko, E. K. Graham, and A. Zalkin, "Optical, mechanical, and thermal properties of barium borate," *J. Appl. Phys.* **62**, 1968–1983 (1987).
14. P. D. Maker, R. W. Terhune, M. Nisenoff, and C. M. Savage, "Effects of dispersion and focusing on the production of optical harmonics," *Phys. Rev. Lett.* **8**, 21–22 (1962).
15. J. Jerphagnon and S. K. Kurtz, "Maker fringes: a detailed comparison of theory and experiment for isotropic and uniaxial crystals," *J. Appl. Phys.* **41**, 1667–1681 (1970).
16. R. W. Terhune, P. D. Maker, and C. M. Savage, "Observation of saturation effects in optical harmonic generation," *Appl. Phys. Lett.* **2**, 54–55 (1963).
17. A. Ashkin, G. D. Boyd, and J. M. Dziedzic, "Observation of continuous optical harmonic generation with gas masers," *Phys. Rev. Lett.* **11**, 14–17 (1963).
18. G. E. Francois, "cw measurement of the optical nonlinearity of ammonium dihydrogen phosphate," *Phys. Rev.* **143**, 597–600 (1966).
19. J. E. Bjorkholm and A. E. Siegman, "Accurate cw measurement of optical second-harmonic generation in ammonium dihydrogen phosphate and calcite," *Phys. Rev.* **154**, 851–860 (1967).

20. J. Ducuing and N. Bloembergen, "Observation of reflected light harmonics at the boundary of piezoelectric crystals," *Phys. Rev. Lett.* **10**, 474–476 (1963).
21. N. Bloembergen, "Second harmonic reflected light," *Opt. Acta* **13**, 311–322 (1966).
22. R. L. Byer and S. E. Harris, "Power and bandwidth of spontaneous parametric emission," *Phys. Rev.* **168**, 1064–1068 (1968).
23. A. J. Campillo and C. L. Tang, "Spontaneous parametric scattering of light in LiIO_3 ," *Appl. Phys. Lett.* **16**, 242–244 (1970).
24. W. N. Herman and L. M. Hayden, "Maker fringes revisited: second-harmonic generation from birefringent or absorbing materials," *J. Opt. Soc. Am. B* **12**, 416–427 (1995).
25. G. D. Boyd and D. A. Kleinman, "Parametric interaction of focused light beams," *J. Appl. Phys.* **39**, 3597–3639 (1968).
26. J. D. Bierlein and F. Ahmed, "Observation and poling of ferroelectric domains in KTiOPO_4 ," *Appl. Phys. Lett.* **51**, 1322–1324 (1987).
27. Y. R. Shen, *The Principles of Nonlinear Optics* (Wiley, New York, 1984), Chap. 9, p. 118.
28. R. L. Byer and R. L. Herbst, "Parametric oscillation and mixing," in *Nonlinear Infrared Generation*, Y.-R. Shen, ed., Vol. 16 of Springer Series in Topics in Applied Physics (Springer-Verlag, Berlin, 1977), pp. 81–137.
29. P. R. Bevington, *Data Reduction and Error Analysis for the Physical Sciences* (McGraw-Hill, New York, 1969), Chap. 11, p. 235.
30. A. V. Smith and M. S. Bowers, "Phase distortions in sum- and difference-frequency mixing in crystals," *J. Opt. Soc. Am. B* **12**, 49–57 (1995).
31. A. V. Smith, W. J. Alford, T. D. Raymond, and M. S. Bowers, "Comparison of a numerical model with measured performance of a seeded, nanosecond KTP optical parametric oscillator," *J. Opt. Soc. Am. B* **11**, 2253–2267 (1995).
32. R. Blachman, P. F. Bordui, and M. M. Fejer, "Laser-induced photochromic damage in potassium titanyl phosphate," *Appl. Phys. Lett.* **64**, 1318–1320 (1994).
33. N. B. Angert, V. M. Garmash, N. I. Pavlova, and A. V. Tarasov, "Influence of color centers on the optical properties of KTP crystals and on the efficiency of laser radiation frequency conversion in these crystals," *Sov. J. Quantum Electron.* **24**, 426–428 (1991).
34. Ref. 27, Chap. 7, p. 86.